A&A 528, A118 (2011)
DOI: 10.1051/0004-6361/201015341

Astronomy & Astrophysics

The influence of temperature on the synthesis of molecules on icy grain mantles in dense molecular clouds

M. Garozzo[1], L. La Rosa[1], Z. Kanuchova[1,2], S. Ioppolo[3], G. A. Baratta[1], M. E. Palumbo[1], and G. Strazzulla[1]

[1] INAF - Osservatorio Astrofisico di Catania, via S. Sofia 78, 95123 Catania, Italy
e-mail: [mga;mepalumbo]@oact.inaf.it
[2] Astronomical Institute of Slovak Academy of Science, 059 60 Tatranska Lomnica, Slovakia
[3] Raymond & Beverly Sackler Laboratory for Astrophysics, Leiden Observatory, Leiden University, PO Box 9513, 2300 RA Leiden, The Netherlands

Received 6 July 2010 / Accepted 2 February 2011

ABSTRACT

Context. Infrared observations show the presence of icy mantles along the line of sight toward young stellar objects (YSOs), where a temperature gradient is expected and indirectly observed. In this environment, icy mantles are affected by ion and UV irradiation. Laboratory experiments show that molecules are formed after irradiation of icy mixtures. However, most of the experiments done so far have been performed in the temperatures range of 10–20 K.
Aims. To extend previous work we irradiated some icy mixtures, namely H_2O:CO=10:1, H_2O:CH_4=4:1, and H_2O:CO_2=3:1 at two different temperatures (12 K and 40 or 60 K) to study the effects of temperature on the synthesis of molecules and the decrease in their parent species after ion irradiation.
Methods. The experiments were performed in a high-vacuum chamber ($P < 10^{-7}$ mbar), where icy samples were irradiated with 30 keV He^+ ions and analyzed by a FTIR spectrophotometer. Infrared spectra of the samples were recorded after various steps of irradiation.
Results. We found that the temperature affects the behavior of the volatile species (i.e., CO and CH_4) during irradiation. As a consequence, the production of molecular species is generally more prevalent at 12 K than at either 40 or 60 K, while the decrease in their parent volatile species is faster at high temperature.
Conclusions. We conclude that the behavior of each species depends on the value of its sublimation temperature with respect to the temperature of the sample. If this latter is higher than the sublimation temperature of a given species, then the effects of thermal desorption compete with those due to irradiation.

Key words. astrochemistry – molecular processes – methods: laboratory – techniques: spectroscopic – ISM: abundances – ISM: molecules

1. Introduction

The nearly empty space between the stars is generally referred to as the interstellar medium (ISM). The ISM consists, 99% in mass, of gas (mainly hydrogen, H) and, 1% in mass, of dust formed by carbonaceous or silicate material as well as polycyclic aromatic hydrocarbons. The ISM is not a uniform environment in neither composition, temperature, nor density. There are locations known as dense molecular clouds (DMCs), where the density of material is relatively high ($>10^4$ n_H cm^{-3}), thus the clouds are optically thick and the temperature can drop as low as 10 K.

Owing to the high density and low temperature of DMCs, gas phase species adhere to the grain surface accreting an ice coating. Atomic hydrogen can thermally move over the ice matrix and eventually react with other atoms or molecules forming simple molecules, primarily water, which is the most abundant species detected, but also methanol (CH_3OH), ammonia (NH_3), and methane (CH_4) (e.g., Hiraoka et al. 1998; Watanabe & Kouchi 2002; Ioppolo et al. 2008; Fuchs et al. 2009; Dulieu et al. 2010). Simultaneously, cosmic ion irradiation produce high-energy processes in the icy mantles, which are deeply chemically and structurally modified. Incoming ions, in fact, release their energy into the target and destroy molecular bonds producing fragments that, by recombination, can form molecules that differ from the original ones and, in general, a modified lattice structure (e.g., Palumbo & Strazzulla 1993; Palumbo et al. 2004; Garozzo et al. 2010). Moreover, DMCs are found in star-forming regions. Close to a forming protostar, high-energy processes in the icy mantles are also induced by the stellar winds and UV photons originating from the protostar itself. During the evolution of a protostar, the temperature of the environment gradually increases, leading to the sublimation of the more volatile species, which enrich the surrounding gas.

Observations of species in the condensed phase provide insight into the chemical and physical processes in these regions. Therefore, the investigation of the relation between the composition and structure of icy mantles and the physical environment is instrumental in understanding the chemical evolution in the envelopes of young stars. Some of the most abundant molecular species detected in the interstellar medium in solid phase, besides H_2O, are CO (which directly condenses from the gas phase), CH_3OH, CH_4, carbonyl sulfide (OCS) and carbon dioxide (CO_2) (e.g., Gibb et al. 2004).

An uncertainty about the chemistry of the ISM concerns the origin of solid CO_2 in the icy mantles on the dust particles. IR

observations of several interstellar clouds show that the abundance of solid CO_2, in polar (water-rich) icy mantles, is in the range 10–25% with respect to water ice, although some sources, e.g., AFGL 989 and Elias 18, exhibit an even higher (34–37%) CO_2 abundance, while CO_2 column density in apolar mantles varies strongly, depending critically on the temperature profile along the line of sight (e.g., Gerakines et al. 1999; Gibb et al. 2004; Boogert et al. 2004; Whittet et al. 2007; Pontoppidan et al. 2008).

Different mechanisms have been proposed for the formation of CO_2 in icy grain mantles. Owing to the low abundance of this molecule in the gas phase (van Dishoeck et al. 1996; Boonman et al. 2003), it is generally accepted that CO_2 is formed on the grain surface via chemical reactions or energetic processing (e.g., Tielens & Hagen 1982; Palumbo & Strazzulla 1993; Stantcheva & Herbst 2004; Fraser & van Dishoeck 2004).

Ruffle & Herbst (2001a) published models of coupled gas-phase and grain surface chemistry that are appropriate for quiescent dense cores. In their models, these authors investigated the effects of grain mantle photodissociation by considering as photon sources the background interstellar and cosmic-ray-induced radiation fields. Relevant photons are those with energy in the 6.9–13.6 eV range (e.g. Jenniskens et al. 1993). These models based on a fixed set of physical conditions, such as a gas and dust temperature of 10 K, reproduce the abundances of solid H_2O and CO observed towards the field star Elias16, but underestimate the abundance of solid CO_2, finding a maximum of 1% with respect to water ice, while the observed abundance is around 23% (Nummelin et al. 2001). Ruffle & Herbst (2001b) developed more complete gas-grain models with a variety of densities and temperatures to determine whether a change in these parameters could enhance the production of CO_2, while preserving the agreement between the predicted and observed abundance of the other major ice components. They found that, in general, an increase in temperature leads to a significant increase in surface CO_2 production because the diffusion rates of the reactants that produce CO_2 become much higher, and competitive reactions involving H atoms become less important as H desorbs more quickly. However, the fraction of CO_2 produced in their models depends strongly also on the physical and chemical conditions adopted, so the results they obtain do not always match the observed CO_2 abundance.

Energetic processing, such as UV ($6.9 \leq E \leq 13.6$ eV) and ion irradiation ($E \sim$ MeV), of icy mantles containing C- and O-bearing species is another possible mechanism of CO_2 production. Laboratory experiments show that CO_2 is formed after the irradiation of pure CO and H_2O:CO ice mixtures (e.g., d'Hendecourt et al. 1986; Moore et al. 1991; Gerakines et al. 1996; Ehrenfreund et al. 1997; Palumbo et al. 1998; Loeffler et al. 2005). Furthermore Mennella et al. (2004, 2006), studied the formation of CO_2 after the irradiation of H_2O on C-grains, and Ioppolo et al. (2009) studied the formation of CO_2 after ion irradiation of ice mixtures illustrating that the amount of CO_2 formed can account for the observed CO_2 in YSOs and that laboratory spectra are good spectroscopic analogues of the interstellar features. Another possible source of C atoms, apart from CO, for accumulating CO_2 in the icy grain mantles can be CH_4, detected via its feature at 7.67 μm in several sources with an abundance in the range 0.3–4% with respect to water ice (Boogert et al. 1997). Irradiation of H_2O:CH_4 mixtures, in fact, easily produce CO_2 (Palumbo et al. 1998).

However, most of the experiments have been performed at low temperature (10–20 K) to mimic the effects of energetic processing in quiescent regions. On the other hand, icy mantles around YSOs are expected to be warmer than 20 K because of the temperature gradient induced by the protostellar object. The presence of the temperature gradient can be inferred from the profile of the 3 μm H_2O band (e.g., Dartois & d'Hendecourt 2001) and the profile of the CO_2 bands (e.g., Gerakines et al. 1999; Ioppolo et al. 2009). Thus, to extend the experimental work presented by Ioppolo et al. (2009) and investigate the possibility that ion irradiation of warm ices increases the CO_2 formation rate as suggested by Ruffle & Herbst (2001b) in the case of photochemistry, we performed new experiments to study the formation of CO_2 (as well as CO) and the decrease of the abundance of the original species after ion irradiation of ice mixtures at higher temperatures (40–60 K). These temperatures are higher than the sublimation temperature of pure CO and CH_4 but these molecules remain on the target because they are embedded in the water ice matrix. The results are compared with those obtained after irradiation of the same mixtures at low temperature (12 K). Details of all the experiments performed and discussed in this work are listed in Table 1.

Table 1. Details of experiments performed and discussed in this work and investigated dose ranges.

Sample	T (K)	Dose range (eV/16 u)
H_2O:CO=10:1	12	0.7–53
H_2O:CO=10:1	40	0.7–30
H_2O:CH_4=4:1	12	0.9–185
H_2O:CH_4=4:1	40	1.4–140
H_2O:CO_2=3:1	12	0.6–49
H_2O:CO_2=3:1	60	0.6–48

Notes. All targets have been irradiated with 30 keV He^+ ions.

2. Experimental apparatus and procedures

The experiments were performed in a high-vacuum chamber ($P < 10^{-7}$ mbar) facing, through KBr windows, a FTIR spectrophotometer (Bruker Equinox 55) working in the spectral range 7500–400 cm^{-1} (1.33–25 μm). Pre-prepared gas mixtures were admitted from a mixing-chamber to the main chamber by a needle valve and accreted in the form of ices on a silicon substrate placed in thermal contact with the tail section of a closed-cycle helium cryostat, whose temperature can vary from 10 to 300 K. Ions were obtained from a 200 kV ion implanter (Danfysik 1080), which is interfaced to the vacuum chamber. The ion beam current densities were maintained below 1 μA cm^{-2} to avoid macroscopic heating of the target. The substrate plane forms an angle of 45° with the IR beam of the spectrometer and the ion beam (the two being mutually perpendicular), so transmittance spectra can be easily obtained in situ, without tilting the sample. After deposition and each step of irradiation, two IR spectra were recorded, selecting the component of the electric vector parallel (P polarization) and perpendicular (S polarization) to the plane of incidence. The polarization was selected using a polarizer placed in the path of the infrared beam in front of the detector. Baratta et al. (2000) and Palumbo et al. (2006) found that when the band profiles recorded in P and S polarization are similar, the features seen in the transmittance spectra directly reflect the variation in the absorption coefficient of the solid sample. This is the case for all the new bands present in our spectra after ion irradiation. Therefore, P spectra were considered in this work since the signal-to-noise ratio is higher for this polarization. However, in the H_2O:CO_2 samples the profile

Table 2. List of the adopted band strength (A) values.

Molecule	Band (cm^{-1})	A (cm molecule^{-1})	Reference
H_2O	3300	2.0×10^{-16}	Allamandola et al. (1988)
CO_2	2345	7.6×10^{-17}	Yamada & Person (1964)
CO	2139	1.1×10^{-17}	Jiang et al. (1975)
CH_4	1303	6.4×10^{-18}	Mulas et al. (1998)

of the CO_2 band at 2344 cm^{-1} in P and S polarization is different, because P spectra show both the longitudinal optical mode (LO) and the transverse optical mode (TO), which lead to LO-TO splitting (Baratta & Palumbo 1998; Palumbo et al. 2006). In these samples, the H_2O band at 3280 cm^{-1} also has a different profile in P and S spectra. In these mixtures, the area of CO_2 and H_2O bands were calculated from S spectra, which display only evidence of the TO mode, because the intensity of the LO mode does not scale linearly with the column density. The profile of the CO band produced after ion irradiation in spectra taken by selecting the P and S components are very similar to each other, therefore, the band area was calculated from P spectra because the signal-to-noise ratio is higher for this case. All spectra shown in the following sections are taken by selecting the P component with a resolution of 1 cm^{-1}.

By measuring the ion fluence (ions cm^{-2}) and using the SRIM software (Ziegler et al. 2008) to calculate stopping powers, we determined, for each experiment, the radiation doses suffered by the target, on a scale of eV per 16 u molecule, where u is the unified atomic mass unit, defined as 1/12 of the mass of an isolated atom of carbon-12.

Satorre et al. (2000) and Ioppolo et al. (2009) demonstrated that the relative abundance of molecules formed after ion irradiation depends on the relative abundance of species present in the initial mixture. Thus, a major concern in the work we present here was to obtain the same mixture at different temperatures. We measured the relative abundance of species in the mixtures after deposition from the integrated intensity of the absorption bands using the band strength values reported in Table 2. As said before, to prepare a sample a pre-prepared gas mixture is admitted into the chamber and the sample is accreted onto the cold substrate in the solid phase. Once all the other parameters are fixed, the deposition rate of each species depends only on the temperature of the substrate. Therefore, if the same gas mixture were prepared in the mixing chamber, the ice mixture obtained would depend on the temperature of the substrate (e.g., Quirico & Schmitt 1997). To obtain ice mixtures with the same relative abundances even at different temperatures, the samples H_2O:CO and H_2O:CO_2 irradiated at 12 K are prepared by depositing the gas mixtures at 40 and 60 K, respectively, and then cooled to 12 K. In the case of the H_2O:CH_4 mixtures, since the accretion rate was calibrated at different temperatures, the samples at 40 and 12 K were prepared by setting gas mixtures with different relative abundances into the mixing-chamber. The thickness of all the samples is of the order of 0.1 μm, which is smaller than the penetration depth of the used ions (30 keV He^+). Therefore, after the energy is released into the material, the He ions are implanted into the silicon substrate on which ices are deposited. For more details of the experimental setup, the reader is referred to Strazzulla et al. (2001).

In all the graphs shown in this paper, we plot the normalized column density of molecular species, which is inferred from the ratio N/N_i where N is the column density (molecules cm^{-2}) of a given species at some point of the irradiation experiment and N_i is the initial column density of the parent molecule. The column density was calculated using the equation:

$$N = \frac{\int \tau_\nu d\nu}{A}, \quad (1)$$

where $\int \tau_\nu d\nu$ (cm^{-1}) is the band area (in an optical depth scale) obtained after subtraction of underlying continuum and A is the band strength (cm molecule^{-1}). The A-values used in this work are listed in Table 2. The column density is corrected by a factor of

$$\cos\theta_r = \sqrt{1 - \frac{\sin^2\theta_i}{n_f^2}}, \quad (2)$$

where θ_r is the refractive angle and n_f is the refractive index of the film. This correction takes into account the longer path length of the IR beam at an incidence angle $\theta_i = 45$ deg (Fulvio et al. 2009; Modica & Palumbo 2010).

Column density values after irradiation are normalized to the initial column density values to compare the results relative to ice samples with slightly different initial thickness.

The experimental data are fitted by using different exponential curves. The decrease in the column density of the species present in the original mixture is described by the exponential curve

$$y = y_\infty + (Y_0 - y_\infty)e^{-\sigma D}, \quad (3)$$

where y is the N/N_i ratio, y_∞ is the asymptotic value of the N/N_i ratio, σ is the cross section in 16 u/eV, D is the dose in eV/16 u, and Y_0 is the extrapolated value of the N/N_i ratio for $D = 0$. This extrapolated value is different from one because of the variation in the band strength of the considered species after irradiation. This variation is due to lattice damage and amorphisation and is almost complete at very low doses, i.e., before the first irradiation step. This assumption is supported by the goodness of the fit obtained. The column density rate (versus fluence) depends on destruction (in the bulk) and sputtering (at the surface). These two processes have a different dependence on the fluence (see e.g. Eq. (4) in Pilling et al. 2010), and their relative contribution depends strongly on the thickness of the sample. In our case, for the thickness used, sputtering is negligible. The formation of a new species is described by the exponential curve

$$y = y_\infty(1 - e^{-\sigma D}), \quad (4)$$

where the same symbolism as in Eq. (3) has been used. In the following, the asymptotic value y_∞ for water represents the fraction of H_2O molecules remaining with respect to the initial H_2O amount. For C-bearing species, it represents the amount remaining (or formed) relative to the amount of the initial C-bearing species. In the literature, G values are often used to describe the formation and destruction of molecules. The G values are defined as the number of molecules produced (destroyed) by an absorbed energy of 100 eV. The G values depend on the irradiation fluence, thus initial yields are usually reported. However, G values can be misleading for astrophysical applications. Laboratory experiments show that new species formed after ion irradiation (and UV photolysis) follow an (almost) linear trend at the beginning of irradiation and then flatten out reaching an equilibrium value. If irradiation proceeds further, new species are destroyed. Thus, if G values are used to estimate the abundance of species produced after irradiation at high fluence, a very large abundance is obtained because G values do not take into account the real trend of new species. We think that the cross-section and asymptotic value are more appropriate to describe the experimental results.

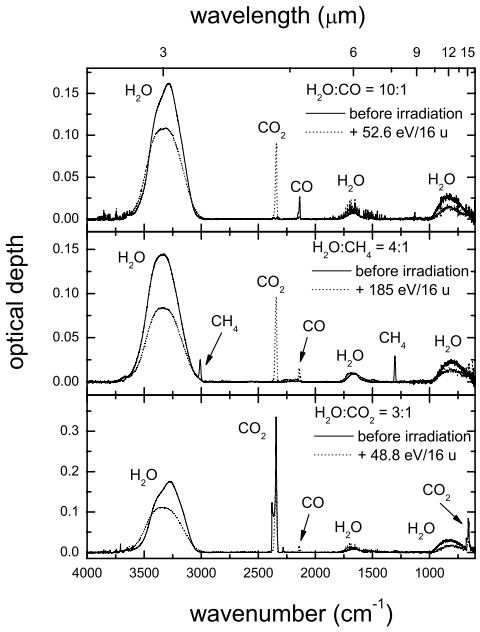

Fig. 1. IR transmittance spectra (in optical depth scale) of the mixtures studied in this work before and after irradiation at 12 K with 30 keV He^+.

Table 3. Peak position of the bands detected in the IR spectra of H_2O:CO=10:1 ice mixture at 12 K and 40 K before and after irradiation.

Wavenumber (cm^{-1})		Molecule
12 K	40 K	
3285	3300	H_2O
2342*	2341*	CO_2*
2137	2136	CO
1660	1678	H_2O
820	824	H_2O
651*	650*	CO_2*

Notes. (*) Detected after irradiation.

3. Results

3.1. Irradiation of H_2O:CO=10:1 mixture at 12 K and 40 K

In the IR transmittance spectra of a thin film of a H_2O:CO=10:1 ice mixture before irradiation at 12 K (Fig. 1 – top panel) and 40 K, the most intense absorption bands observed at about 3300, 1660, and 820 cm^{-1} are due to solid water ice, while the band at about 2136 cm^{-1} is due to CO ice.

After irradiation with 30 keV He^+, in both samples, the intensity of these bands decreases and two new bands, amenable to CO_2, are detected at 2342 and 650 cm^{-1} (see e.g., Moore et al. 1991). The peak position and identification of the bands detected in the samples at 12 K and 40 K before and after irradiation are listed in Table 3.

The values of the normalized column density of H_2O, CO, and CO_2 during irradiation, in the samples at both temperatures are plotted in Fig. 2. Column density values after irradiation are normalized to the initial column density values in order to compare the results relative to ice samples with slightly different initial thickness.

Water column densities at 12 K and 40 K decrease slowly and only in the first steps of irradiation. At around 30 eV/16 u, the water column density is 80–90% of its initial value, and appears to be unaffected by the temperature. These trends are

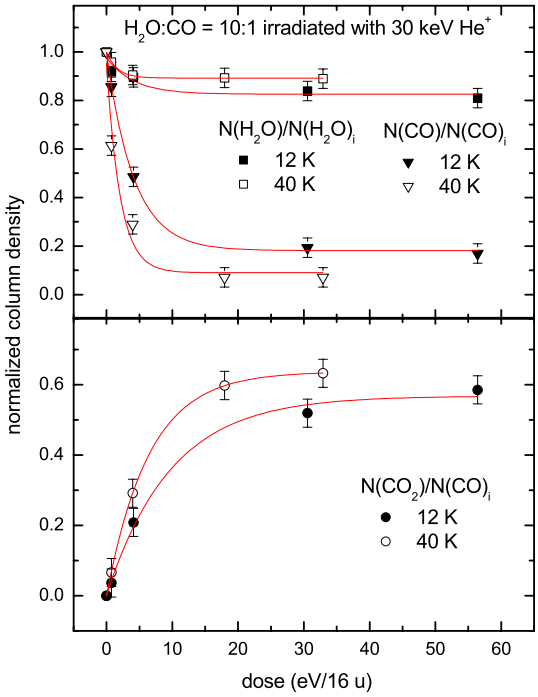

Fig. 2. Trend of the normalized column density of H_2O, CO, and CO_2 in the sample H_2O:CO=10:1 irradiated with 30 keV He^+ at 12 K and 40 K, and their fit.

fitted by using Eq. (3) with the values of the parameters listed in Table 4.

We irradiated thin films of pure water ice at temperatures lower than 80 K and found that water has a very low destruction yield. Most of the dissociated molecules react to reform water and the water column density becomes about 95% of its initial value (Gomis et al. 2004). The destruction include both molecules sputtered away from the target and molecules processed to form H_2O_2, which is identifiable from the band at about 2850 cm^{-1}. In the present experiments, we found a slightly higher destruction yield and we conclude that the presence of other species in the mixture (such as CO) supports the formation of new molecules providing an alternative pathway to the reaction that reforms the water. This increases the destruction yield of water at temperatures lower than its sublimation temperature (about 160 K). In particular, in the case of the H_2O:CO mixture irradiated at 12 K, the amount of CO_2 formed is about 60% of the original CO. After irradiation of pure CO (Ioppolo et al. 2009), the amount of CO_2 formed is about 10% of the original CO. By comparing these results, it is evident that H_2O plays a relevant role in the formation of CO_2. We estimated that the decrease in H_2O column density is compatible with the increase in CO_2 column density.

The CO column density, at the end of the experiment at 12 K is reduced to 20% of its initial value, while by the end of irradiation performed at 40 K it has become 10%. In both experiments, 60% of CO was oxygenated to form CO_2, while the remainder was sputtered, thermally desorbed, or used to form minor species not detected in our spectra and a carbon-rich residue. The data of CO column densities are fitted by using Eq. (3) with values listed in Table 4. The trends of the CO_2 formation at the two temperatures are very similar and the CO_2 normalized column density reaches, at the end of irradiation, the value of 60% with respect to the initial CO, in both samples. To fit these data, Eq. (4) was used with the values listed in Table 4. Hence, the

Table 4. Best-fit parameters following the fitting of the experimental data related to the samples H_2O:CO=10:1 at 12 K and 40 K with Eqs. (3) and (4).

	$(Y_0 - y_\infty)$		σ(16 u/eV)		y_∞	
	12 K	40 K	12 K	40 K	12 K	40 K
H_2O	0.15 ± 0.04	0.11 ± 0.01	0.51 ± 0.37	0.61 ± 0.08	0.83 ± 0.02	0.89 ± 0.01
CO	0.81 ± 0.01	0.86 ± 0.10	0.24 ± 0.01	0.55 ± 0.19	0.18 ± 0.01	0.09 ± 0.06
CO_2			0.10 ± 0.02	0.15 ± 0.02	0.57 ± 0.03	0.64 ± 0.03

Table 5. Peak position of the bands detected in the IR spectra of H_2O:CH_4=4:1 ice mixture as deposited at 12 K and 40 K and after irradiation.

Wavenumber (cm^{-1})		Molecule
12 K	40 K	
3300	3291	H_2O
3010	3009	CH_4
2975	2976*	C_2H_6*
2341	2341*	CO_2*
2137	2136*	CO*
1680	1663	H_2*O
1500	1497*	H_2CO*
1301	1301	CH_4
1017	1017*	CH_3OH
807	806	H_2O

Notes. (*) Detected after irradiation.

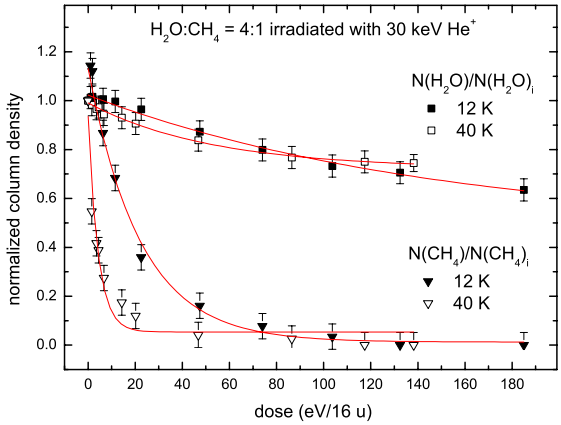

Fig. 3. Trend of the column density of the parent molecules in the mixture H_2O:CH_4=4:1 during irradiation with 30 keV He^+ at 12 K and 40 K and their fit.

higher cross-section for disappearance of CO at 40 K is probably due to its desorption and not to a more efficient dissociation of this molecule. The role of temperature in these samples became evident when we considered that the ratio H_2O:CO increased from 10:1 before irradiation to 40:1 at the end of irradiation at 12 K and to 140:1 at the end of irradiation at 40 K.

3.2. Irradiation of H_2O:CH_4 = 4:1 mixture at 12 K and 40 K

Figure 1 (middle panel) shows the IR spectra of a thin film of H_2O:CH_4=4:1 ice mixture deposited at 12 K together with the IR spectrum of the same sample after irradiation with 30 keV He^+. These spectra are similar to those of the sample prepared and irradiated at 40 K. The irradiation of these mixtures led to the production of several new molecules, mainly CO_2 but also CO, ethane (C_2H_6), formaldehyde (H_2CO), and methanol (CH_3OH) (see e.g., Baratta et al. 2003). Peak positions and the identification of the bands detected before and after irradiation can be found in Table 5. All the bands clearly present in the spectra are included in the table. From other experiments (e.g. Baratta et al. 2003), we know that other species (such as C_3H_8 and C_2H_4) are formed after the irradiation of H_2O:CH_4 mixtures. However, because of the lower thickness of the samples in the present experiments the bands corresponding to these species are not evident in the spectra.

The normalized column densities of H_2O and CH_4 at 12 K and 40 K are plotted as a function of the dose in Fig. 3. To fit these data, Eq. (3) was used with the parameter values listed in Table 6.

In these mixtures, the water column density decreases slowly with irradiation and at 12 K has not reached the asymptotic value even at the highest investigated dose. At a dose of 140 eV/16 u, the value of the water column density is around 70% of its initial value at both considered temperatures. We note that the normalized water column density is higher than one at the beginning of irradiation at 12 K. This is not a real growth but an effect of the variation in the band strength of the 3 μm band of water ice during irradiation as studied by Leto & Baratta (2003).

At 12 K, the CH_4 normalized column density value has a very prompt drop off at the beginning of irradiation and is less than 20% of its initial value at around 40 eV/16 u dose. At 40 K, this process appears to be very rapid as the ratio σ(40 K)/σ(12 K) = 5 (see Table 6) clearly indicates. Furthermore, at the end of both experiments, CH_4 is undetectable at both temperatures. In the first steps of irradiation at 12 K, the normalized column density of CH_4 is higher than one. As in the case of water ice previously described, this is due to the variation in the band strength value as discussed in Leto & Baratta (2003) and Loeffler et al. (2005).

The ratio H_2O:CH_4 changes significantly after irradiation. The initial ratio 4:1 has increased to 90:1 by the end of irradiation at 12 K and to more than 105:1 by the end of irradiation at 40 K.

The trend of the CO_2 formation as a function of dose at 12 K and 40 K is shown in Fig. 4. The formation of CO_2 molecules is more effective at low temperature as becomes evident at irradiation doses higher than 40 eV/16 u. At the highest investigated dose, the maximum ratio of the produced CO_2 to the initial CH_4 is 40%.

Owing to the change in the CO_2 production rate at a "threshold dose D_0" of about 20 eV/16 u, the trend of CO_2 column density at 12 K is fitted with two exponential curves. In detail,

$$y = y_1(1 - e^{-\sigma_1 D}) \quad \text{when} \quad D \le D_0 \qquad (5)$$

$$y = y_1(1 - e^{-\sigma_1 D}) + y_2[1 - e^{-\sigma_2 (D - D_0)}] \quad \text{when} \quad D > D_0 \qquad (6)$$

where y_1 and y_2 are the asymptotic values, σ_1 and σ_2 are the cross-sections, and D is the dose. The values of these parameters are listed in Table 7. The production rate of CO_2 at 40 K could

Table 6. Best-fit parameters following the fitting of the experimental data related to the samples H_2O:CH_4=4:1 at 12 K and 40 K with Eq. (3).

	$(Y_0 - y_\infty)$		σ(16 u/eV)		y_∞	
	12 K	40 K	12 K	40 K	12 K	40 K
H_2O	0.55 ± 0.07	0.27 ± 0.01	$(7.04 \pm 1.49) \times 10^{-3}$	$(1.86 \pm 0.20) \times 10^{-2}$	0.47 ± 0.07	0.72 ± 0.01
CH_4	1.12 ± 0.05	0.88 ± 0.07	$(4.58 \pm 0.62) \times 10^{-2}$	0.24 ± 0.04	0.01 ± 0.03	0.05 ± 0.04

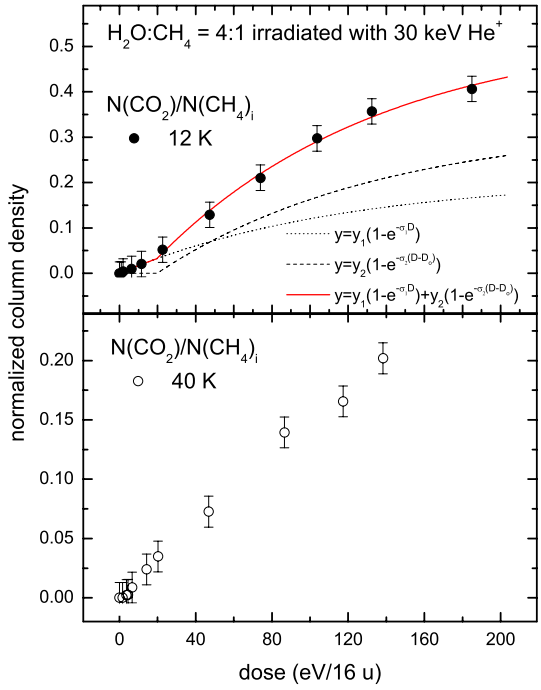

Fig. 4. Trend of the normalized column density of CO_2 synthesized in the mixture H_2O:CH_4=4:1 at various steps of irradiation and at two different temperatures. For 12 K, the fit is also shown.

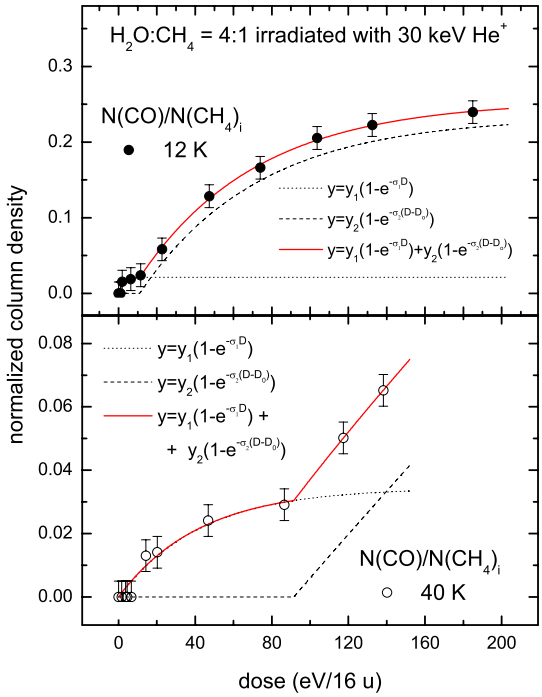

Fig. 5. Trend of the normalized column density of CO formed in the mixture H_2O:CH_4=4:1 at various steps of irradiation and at two different temperatures together with the fit.

be fitted with a straight line, given by the relation $y = y_1 \times \sigma_1 \times D$, so only the product $y_1 \times \sigma_1$ could be evaluated.

The formation of CO molecules as a function of the dose is shown in Fig. 5. The CO formation is quite effective at 12 K, reaching 25% of initial CH_4, while at 40 K the CO abundance remains less than 10% of initial CH_4 during the experiment, hence in this case, temperature also plays a significant role.

As for CO_2 at 12 K, the trend of CO was fitted with the two exponential curves described by Eqs. (5) and (6) with the parameter values listed in Table 7. In the case of the curve that fits the CO trend at 40 K for $D > D_0$, a straight line is produced by the fitting procedures. Developing the exponential in a Mac Laurin series and stopping it at the first order, the equation is approximated by the relationship $y = \sigma_2 \times y_2 \times (D - D_0)$, which is the equation of a straight line. Thus, it is impossible to calculate separately σ_2 and y_2 since the fitting procedure depends only on their product.

After irradiation, the column density of water and methane decreases, while the column density of newly formed species, such as CO and CO_2, increases. We note that at low doses the trend of CO and CO_2 production differs from that at higher doses. Furthermore, at low doses, the main molecules formed are hydrocarbons (Baratta et al. 2002), whose column density decreases at higher doses when the CO and CO_2 column densities increase. First and second generation molecules therefore exist. The presence of newly formed solid CO in the mixture is consistent with CO_2 synthesis, because reactions with CO as a precursor, such as CO + OH, are significant. In addition, CO_2 could be formed by reactions that do not have CO as a precursor. In particular, Ferini et al. (2004) and Palumbo et al. (2004) demonstrated that a refractory organic residue is formed after irradiation of CH_4-bearing icy mixtures. We consider this residue to be a C reservoir that contributes to the formation of CO and CO_2 at high doses. We performed several blank experiments (see e.g. Mennella et al. 2004; and Strazzulla et al. 2003) irradiating pure water ice, which show that CO and CO_2 contamination is negligible.

3.3. Irradiation of H_2O:CO_2=3:1 mixture at 12 K and 60 K

The last experiments described in this paper concern the irradiation of two icy mixtures H_2O:CO_2=3:1 at 12 K and 60 K. The spectrum of the sample at 12 K before and after irradiation is shown in Fig. 1 (bottom panel). The main difference between these two spectra is the decrease in the intensity of the band areas of H_2O and CO_2 and the appearance of a new band due to CO at 2141 cm^{-1}. After irradiation, CO is not the only molecular species that we detected: we also detect carbon trioxide (CO_3), ozone (O_3), hydrogen peroxide (H_2O_2), and carbonic acid (H_2CO_3) (see e.g., Strazzulla et al. 2005). The peak positions and identification of the molecular species detected in the mixtures at 12 K and 60 K before and after irradiation are listed in Table 8.

Table 7. Best-fit parameters following the fitting of the experimental data related to CO and CO_2 formed after irradiation of the sample H_2O:CH_4=4:1 at 12 K and 40 K with Eqs. (5) and (6).

	D_0 (eV/16 u)	y_1	σ_1 (16 u/eV)	y_2	σ_2 (16 u/eV)
CO_2 (12 K)	19 ± 3	0.21 ± 0.01	$(8.7 \pm 2.0) \times 10^{-3}$	0.33 ± 0.01	$(8.8 \pm 3.8) \times 10^{-3}$
CO (12 K)	11 ± 3	$(2.1 \pm 0.8) \times 10^{-2}$	0.37 ± 0.31	0.23 ± 0.01	$(1.6 \pm 0.2) \times 10^{-2}$
CO (40 K)	91 ± 5	$(3.4 \pm 2.0) \times 10^{-2}$	$(2.3 \pm 1.0) \times 10^{-2}$		

Table 8. Peak position of the bands detected in the IR spectra of H_2O:CO_2=3:1 ice mixture at 12 K and 60 K before and after irradiation.

Wavenumber (cm^{-1}) 12 K	60 K	Molecule
3708	3707	CO_2
3589	3599	CO_2
3274	3280	H_2O
2850*	2856*	H_2O_2*
2344	2344	CO_2
2282	2281	$^{13}CO_2$
2141*	2139*	CO*
2045*	2045*	CO_3*
1664	1669	H_2O
1500*	1497*	H_2CO_3*
1309*	1301*	H_2CO_3*
1038*	1040*	O_3*
836	836	H_2O
660	657	CO_2

Notes. (*) Detected after irradiation.

In Fig. 6, the trends of the normalized column density of H_2O, CO_2, and CO at 12 K and 60 K are plotted as a function of the dose. Equation (3) is used to fit the H_2O and CO_2 data, while Eq. (4) is used to fit the CO data. The values of the parameters used in these equations are listed in Table 9.

In these experiments, water exhibits a different behavior with temperature; at 12 K, its column density suddenly decreases during the first step of irradiation to 85%, a value close to the asymptotic value. At 60 K, the water column density decreases with a more uniform behavior during irradiation, reaching 85% of its initial value at high doses. The CO_2 column density is unaffected by temperature, and it decreases almost in the same way at both temperatures reaching a value around 50% of the initial CO_2 value at high doses. The ratio H_2O:CO_2 increased from the initial 3:1 ratio before irradiation to a final 4:1 at 12 K and 5:1 at 60 K. These results show how the temperature does not play a significant role in this case. The CO column density also shows a similar behavior at both temperatures. It increases rapidly and reaches saturation at a dose higher than 15 eV/16 u. However, there is a small difference in the amount of CO produced at different temperatures: 20% of initial CO_2 at 12 K and 12% at 60 K. The minor amount of CO at 60 K is most likely due to its desorption.

4. Discussion

We have performed a set of experiments designed to the study of the formation of CO_2 and CO and the decrease in the original species after the ion irradiation of various icy mixtures at different temperatures. In detail, H_2O:CO=10:1 and H_2O:CH_4=4:1 mixtures were irradiated at 12 K and 40 K. We found that the decrease in CO and CH_4 is faster at 40 K, which is a

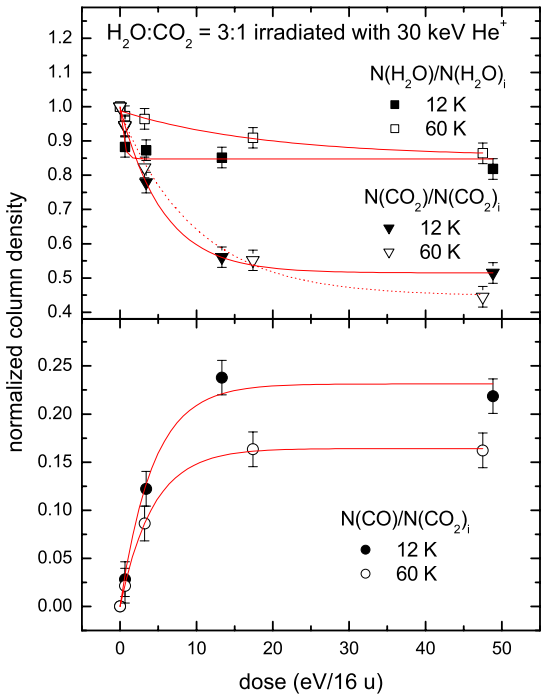

Fig. 6. Trend of H_2O, CO_2, and CO column density at various steps of irradiation of the sample H_2O:CO_2=3:1 at two different temperatures together with their fit.

temperature higher than their sublimation temperature (~30 K), rather than at 12 K. The difference is higher for the CH_4 molecules. The H_2O:CO_2=3:1 mixture was irradiated at 12 K and 60 K, which are values lower than the sublimation temperature of CO_2 (~90 K). The trend of CO_2 destruction at both temperatures is the same within the error of the measurement.

In the mixtures with CO and CO_2, the water column density decreases when subjected to low doses of irradiation and immediately reaches an asymptotic value in the range of 80–90% of its initial value. For mixtures containing CH_4, the water column density decreases during the whole irradiation process without reaching an asymptotic value even at high doses.

We irradiated thin films of pure water ice at temperatures lower than 80 K and found that water has a very low destruction yield and that at the end of the experiments, the water column density was about 95% of its initial value (Gomis et al. 2004). The destruction include both molecules sputtered away from the target and molecules processed to form H_2O_2, which is identified from the band at about 2850 cm^{-1}. In the present experiments, we found a slightly higher destruction yield and conclude that the presence of other species in the mixture (such as CO, CO_2, and CH_4) promotes the formation of new molecules and increases the destruction yield of water at temperatures lower than its sublimation temperature (about 160 K). In the case of H_2O:CH_4 mixtures, a C-rich refractory residue is formed after

Table 9. Best-fit parameters following the fitting of the experimental data related to the samples H_2O:CO_2=3:1 at 12 K and 60 K with Eqs. (3) and (4).

	$(Y_0 - y_\infty)$		σ(16 u/eV)		y_∞	
	12 K	60 K	12 K	60 K	12 K	60 K
H_2O	0.15 ± 0.03	0.13 ± 0.02	3.60 ± 2.15	0.07 ± 0.03	0.85 ± 0.02	0.85 ± 0.02
CO_2	0.48 ± 0.01	0.54 ± 0.02	0.18 ± 0.01	0.10 ± 0.02	0.51 ± 0.01	0.45 ± 0.02
CO			0.23 ± 0.04	0.23 ± 0.01	0.23 ± 0.01	0.16 ± 0.01

irradiation (e.g. Ferini et al. 2004; Palumbo et al. 2004). This residue is a source of carbon and explains the formation of CO and CO_2 and the destruction of water at high doses when almost no CH_4 is left in the sample.

The formation of CO and CO_2 is directly related to the type of irradiated mixtures. The formation of CO_2 after irradiation of H_2O:CO mixtures is slightly temperature dependent, but strongly depends on the temperature when H_2O:CH_4 mixtures are irradiated. Moreover, the formation of CO after the irradiation of the H_2O:CH_4 and H_2O:CO_2 mixtures is also temperature dependent and more likely at lower temperatures (12 K). The production cross-section of CO_2 is higher in the mixture H_2O:CO, where the value of the CO_2 column density reaches saturation after ~30 eV/16 u at both temperatures, while in the mixture H_2O:CH_4 the saturation of CO_2 column density is not reached in any case, even at the higher investigated doses. Similarly the CO column density reaches the saturation value after irradiation of the mixture H_2O:CO_2, while in the mixture H_2O:CH_4 the CO molecules are synthesized even at doses higher than 140 eV/16 u. However, in this mixture at 12 K and 40 K, at doses higher than 80 eV/16 u, CH_4 is almost totally destroyed, and the production of CO and CO_2 can proceed only because of the presence of a C-rich residue. The formation of an organic residue after the ion irradiation of icy mixtures containing C-, H-, and O-bearing species is supported by several laboratory investigations (e.g., Ferini et al. 2004).

Our experimental results show that the fate of the volatile species, such as CO and CH_4, is strongly dependent on the temperature. The CO_2 production is not strongly affected by temperature in H_2O:CO mixtures, but in the case of H_2O:CH_4 mixtures the production of CO and CO_2 is less efficient at higher temperatures. Therefore, although an increase in temperature increases the diffusion rates of the reactants that produce CO_2, it does not enhance the efficiency of its production. Thermal desorption of the CO and CO_2 precursor species tends to inhibit the formation process of the final products.

5. Astrophysical applications

In dense molecular clouds ($>10^4$ n_H cm^{-3}), gas phase species condense on grains forming icy mantles. Some species (such as CO) directly freeze out from the gas phase, while other molecules (such as H_2O) are formed after grain surface reactions. Icy mantles have been observed in quiescent regions along the line of sight toward field stars (e.g., Chiar et al. 1994, 1995; Whittet et al. 1998) and along the line of sight toward YSOs (Tielens et al. 1991; Gerakines et al. 1999; Gibb et al. 2004; Pontoppidan et al. 2008). A detailed study of the absorption profile of observed bands indicates that annealing occurs in icy mantles around YSOs (Gerakines et al. 1999; Dartois & d'Hendecourt 2001; Pontoppidan et al. 2008). Icy mantles are continuously exposed to energetic processes such as low-energy cosmic-ray irradiation and UV photolysis and these alter both the chemical and the lattice structure of the target material with the formation of molecular species. It has been estimated that the proton flux, following the approximation of monoenergetic 1 MeV protons, has a value of 1.8 protons cm^{-2} s^{-1} in diffuse quiescent regions and 1 proton cm^{-2} s^{-1} in dense quiescent regions (Mennella et al. 2003). The UV flux under diffuse medium conditions has been estimated as 8×10^7 photons cm^{-2} s^{-1} (Mathis et al. 1983). In dense regions, the internal UV flux due to cosmic-ray induced fluorescence of molecular hydrogen ranges from 1.4×10^3 to 4.8×10^3 photons cm^{-2} s^{-1} (Prasad & Tarafdar 1983; Mennella et al. 2003). Considering the amount of energy released by ions and photons passing through an ice mantle, the effects of UV photons would dominate in diffuse regions while the effects of ions and UV photons are comparable in dense regions (Moore, 1999). Greenberg (1982) estimated that the lifetime of a dense cloud is in the interval 3×10^7–5×10^8 years. Assuming a density of $n = 10^4$ n_H cm^{-3}, $10^9/n \sim 10^5$ years are needed for gas to condense onto grains (Tielens & Allamandola 1987). Thus, icy grain mantles are irradiated for a time that ranges from 10^5 years (the grain mantles sublime immediately after the formation) to 5×10^8 years (the icy grain mantles survive for all the cloud lifetime). The specific energy loss (stopping power) of 1 MeV protons into a typical grain containing heavy atoms (C, N, O, Si) is $\sim 5 \times 10^{-15}$ eV cm^2 atom^{-1}. The energy deposited on a grain (dose), given by the product of the stopping power, the flux, and the mantle lifetime is around 0.015–75 eV/atom (C, N, O, Si). In star-forming regions, the flux of ions due to stellar flares must also be considered. This flux was estimated by Strazzulla et al. (1983) to be 200 protons cm^{-2} s^{-1}, so the energy deposited onto a grain in 10^6 years (a YSO lifetime) is around 30 eV/atom (C, N, O, Si). Mixtures studied in this work were irradiated with a dose in the range 0.6–185 eV/16 u, which is comparable with the higher values of doses absorbed by icy mantles.

Our experimental results show that the formation of molecular species does not depend on the temperature while the temperature of the sample is lower than the sublimation temperature of the investigated species. On the basis of our results, we expect that the amount of CO_2 formed during the YSO stage is comparable to the amount formed in quiescent regions. The dose suffered by icy mantles in quiescent regions is indeed comparable to the dose suffered during the YSO stage.

Ruffle & Herbst (2001a,b) published models of coupled gas-phase and grain surface chemistry. In these models, the effects of grain mantle photodissociation were investigated by considering as photon sources the background interstellar and cosmic-ray-induced radiation fields. They found that, in general, an increase in temperature leads to a significant increase in surface CO_2 production because the diffusion rates of the reactants that produce CO_2 become much higher and competitive reactions involving H atoms become less important as H desorbs more quickly. If we assume that the effects of photons and fast ions are the same, the experimental results presented here do not support their finding. However, this conclusion needs more experimental work to be confirmed. The comparison between experimental results

and models is not straightforward. Furthermore, Ruffle & Herbst (2001a,b) consider the effects of photons that, in principle, could behave differently from fast ions (see e.g. Baratta et al. 2002).

Finally we note that the observed abundance of CH_4 is about 1–4% with respect to water towards high-mass YSOs (Gibb et al. 2004; Boogert et al. 1997) and about 2–8% towards low-mass YSOs (Öberg et al. 2008). In particular, the model by Ruffle & Herbst (2001a), which takes into account photochemistry, predicts a value of CH_4 higher than 10% with respect to water ice, which is higher than the observed values. On the basis of our experimental results, we suggest that cosmic-ion and UV irradiation could contribute to the destruction and consequently to the low abundances of CH_4 in icy grain mantles.

Acknowledgements. We thank F. Spinella for his help in the laboratory. This research has been supported by Italian Space Agency contract No. I/015/07/0 (Studi di Esplorazione del Sistema Solare) and by the European Community's Seventh Framework Programme (FP7/2007-2013 under grant agreement No. 238258).

References

Allamandola, L. J., Sandford, S. A., & Valero, G. J. 1988, Icarus, 76, 225
Baratta, G. A., & Palumbo, M. E. 1998, J. Opt. Soc. Am. A, 15, 3076
Baratta, G. A., Palumbo, M. E., & Strazzulla, G. 2000, A&A, 357, 1045
Baratta, G. A., Leto, G., & Palumbo, M.E. 2002 A&A, 384, 343
Baratta, G. A., Domingo, M., Ferini, G., et al. 2003, NIMB, 209, 283
Boogert, A. C. A., Schutte, W. A., Helmich, F. P., Tielens, A. G. G. M., & Wooden, D. H. 1997, A&A, 317, 929
Boogert, A. C. A., Pontoppidan, K. M., Lahuis, F., et al. 2004, ApJS, 154, 359
Boonman, A. M. S., van Dishoeck, E. F., Lahuis, F., & Doty, S. D. 2003, A&A, 399, 1063
Chiar, J. E., Adamson, A. J., Kerr, T. H., & Whittet, D. C. B. 1994, ApJ, 426, 240
Chiar, J. E., Adamson, A. J., Kerr, T. H., & Whittet, D. C. B. 1995, ApJ, 455, 234
Dartois, E., & d'Hendecourt, L. 2001, A&A, 365, 144
Dulieu, F., Amiaud, L., Congiu, E., et al. 2010, A&A, 512, A30
d'Hendecourt, L. B., Allamandola, L. J., Grim, R. J. A., & Greenberg, J. M. 1986, A&A, 158, 119
Ehrenfreund, P., Boogert, A. C. A., Gerakines, P. A., Tielens, A. G. G. M., & van Dishoeck, E. F. 1997, A&A, 328, 649
Ferini, G., Baratta, G. A., & Palumbo, M. E. 2004, A&A, 414, 757
Fraser, H. J., & van Dishoeck, E. F. 2004, Adv. Space Res., 33, 14
Fuchs, G. W., Cuppen, H. M., Ioppolo, S., et al. 2009, A&A, 505, 629
Fulvio, D., Sivaraman B., Baratta, G.A., et al. 2009, Spectrochimica Acta A, 72, 1007
Garozzo, M., Fulvio, D., Kanuchova, Z., Palumbo, M. E., & Strazzulla, G. 2010, A&A, 509, A67
Gerakines, P. A., Schutte, W. A., & Ehrenfreund, P. 1996, A&A, 312, 289
Gerakines, P. A.,Whittet, D. C. B., Ehrenfreund, P., et al. 1999, ApJ, 522, 357
Gibb, E. L., Whittet, D. C. B., Boogert, A. C. A., & Tielens, A. G. G. M. 2004, ApJS, 151, 35
Gomis, O., Leto, G., & Strazzulla, G. 2004, A&A, 420, 405
Greenberg, M. 1982, in Comets, ed. L.L. Wilkening (Tucson: The University of Arizona Press), 131
Hiraoka, K., Miyagoshi, T., Takayama, T., Yamamoto, K., & Kihara, Y. 1998, ApJ, 498, 710
Ioppolo, S., Cuppen, H. M., Romanzin, C., van Dishoeck, E. F., & Linnartz, H. 2008, ApJ, 686, 1474
Ioppolo, S., Palumbo, M. E., Baratta G. A., & Mennella, V. 2009, A&A, 493, 1017
Jenniskens, P., Baratta, G. A., Kouchi, A., et al. 1993, A&A, 273, 583
Jiang, G. J., Person, W. B., & Brown, K. G. 1975, J. Chem. Phys., 62, 1201
Leto, G., & Baratta, G. A. 2003, A&A, 397, 7
Loeffler, M. J., Baratta, G. A., Palumbo, M. E., Strazzulla, G., & Baragiola, R. A. 2005, A&A, 435, 587
Mathis, J. S., Mezger, P. G., & Panagia, N. 1983, A&A, 128, 212
Mennella, V., Baratta, G. A., Esposito, A., Ferini, G., & Pendleton, Y. J. 2003, ApJ, 587, 727
Mennella, V., Palumbo, M. E., & Baratta, G. A. 2004, ApJ, 615, 1073
Mennella, V., Baratta, G. A., Palumbo, M. E., & Bergin, E. A. 2006, ApJ, 643, 923
Modica, P., & Palumbo, M. E. 2010, A&A, 519, A22
Moore, M. H. 1999, in Solid Interstellar Matter: the ISO Revolution, ed. L. d'Hendecourt, C. Joblin, & A. Jones (New York: Springer-Verlag), 199
Moore, M. H., Khanna, R., & Donn, B. 1991, J. Geophys. Res., 96, 17541
Mulas, G., Baratta, G. A., Palumbo, M. E., & Strazzulla, G. 1998, A&A, 333, 1025
Nummelin, A., Whittet, D. C. B., Gibb, E. L., Gerakines, P. A., & Chiar, J. E. 2001, ApJ, 558, 185
Öberg, K., Boogert, A. C. A., Pontoppidan, K. M., et al. 2008, ApJ, 678, 1032
Palumbo, M. E., & Strazzulla, G. 1993, A&A, 269, 568
Palumbo, M. E., Baratta, G. A., Brucato, J. R., et al. 1998, A&A, 334, 247
Palumbo, M. E., Ferini, G., & Baratta, G. A. 2004, Adv. Sp. Res., 33, 49
Palumbo, M. E., Baratta, G. A., Collings, M. P., & McCoustra, M. R. S. 2006, Phys. Chem. Chem. Phys., 8, 279
Pilling, S., Seperuelo Duarte, E., da Silveira, E. F., et al. 2010, A&A, 509, A87
Pontoppidan, K. M., Boogert, A. C. A., Fraser, H. J., et al. 2008, ApJ, 678, 1031
Prasad, S. S., & Tarafdar, S. P. 1983, ApJ, 267, 603
Quirico, E., & Schmitt, B. 1997, Icarus, 127, 354
Ruffle, D. P., & Herbst, E. 2001a, MNRAS, 322, 770
Ruffle, D. P., & Herbst, E. 2001b, MNRAS, 324, 1054
Satorre, M. A., Palumbo, M. E., & Strazzulla, G. 2000, Ap&SS, 274, 643
Stantcheva, T., & Herbst, E. 2004, A&A, 423, 241
Strazzulla, G., Calcagno, L., & Foti, G. 1983, MNRAS, 204, 59
Strazzulla, G., Baratta G. A., & Palumbo M. E. 2001, Spectrochim. Acta, 57, 825
Strazzulla, G., Leto, G., Gomis, O., & Satorre, M. A. 2003, Icarus, 164, 163
Strazzulla, G., Leto, G., Spinella, F., & Gomis, O. 2005, AsBio, 5, 612
Tielens, A. G. G. M., & Allamandola, L. J. 1987, ASSL, 134, 397
Tielens, A. G. G. M., & Hagen, W. 1982, A&A, 114, 245
Tielens, A. G. G. M., Tokunaga, A. T., Geballe, T. R., & Baas, F. 1991, ApJ, 381, 181
van Dishoeck, E. F., Helmich, F. P., de Graauw, T., et al. 1996, A&A, 315, L349
Watanabe, N., & Kouchi, A. 2002, ApJ, 571, L173
Whittet, D. C. B., Gerakines, P. A., Tielens, A. G. G. M., et al. 1998, ApJ, 498, L159
Whittet, D. C. B., Shenoy, S. S., Bergin, E. A., et al. 2007, ApJ, 655, 332
Yamada, H., & Person, W. B. 1964, J. Chem. Phys., 41, 2478
Ziegler J. F., Biersack, J. P., & Ziegler M. D., 2008, The stopping and range of ions in solids (New York: Pergamon Press), see also `http://www.srim.org`